Model of the amplified spontaneous emission generation in thulium-doped silica fibers

Martin Gorjan,* Thibault North, and Martin Rochette

Department of Electrical and Computer Engineering, McGill University, 3480 University St. Montreal, Quebec H3A 2A7, Canada

**Corresponding author: martin.gorjan@mcgill.ca*

Received May 16, 2012; revised August 6, 2012; accepted August 28, 2012; posted August 28, 2012 (Doc. ID 168695); published September 24, 2012

A model of the ~2 μm amplified spontaneous emission (ASE) generation in the thulium-doped silica fibers pumped at 1575 nm is presented. Both Al-codoped and Al/Ge-codoped fiber core compositions are studied. The results show that the composition affects the relative slope efficiency of 10% and the bandwidth of 19% of the output ASE. Our results predict that the backward ASE is more powerful and spectrally broader compared to the forward ASE, which is in agreement with previous experiments. Using an asymmetric cavity feedback, 98% of the total output power can be directed in the backward ASE, but with the consequence of losing ~50% of the bandwidth. Such sources are expected to deliver single-mode output with more than 70% slope and 39% power conversion efficiency.

OCIS codes: 140.3070, 140.3510, 140.5680, 140.6630.

1. INTRODUCTION

Broadband sources in the spectral region near 2 μm can be of great interest for applications ranging from spectroscopy and gas sensing [1] to low coherence interferometry and medical imaging with optical coherence tomography [2]. An attractive way to produce such broadband light is using an amplified spontaneous emission (ASE) on the $^3F_4 \rightarrow {}^3H_6$ transition from a thulium (Tm) doped silica fiber [3]. This transition has been well studied theoretically for different pumping regimes in lasers, fiber amplifiers, and double-clad fiber lasers with ring cavity [4–6]. It has been determined that high efficiency of laser operation can be attained by diode pumping on the transition $^3H_6 \rightarrow {}^3H_4$ in combination with high Tm-doping concentrations that enable beneficial interionic cross-relaxations [7]. Alternatively, by pumping directly to the upper laser level on the transition $^3H_6 \rightarrow {}^3F_4$, the need for high doping concentrations can be avoided. Nevertheless, high efficiencies can still be attained because of the much lower quantum defect associated with this so-called inband pumping. This was recently demonstrated experimentally, where the authors reported 37% slope efficiency in single-frequency [8], 50% in gain-switch [9], and 80% in *Q*-switch operation regimes [10].

Studies of the ASE operation, however, have been much scarcer. A Tm-Ho-codoped fiber was pumped both at 1610 nm and also at 803 nm producing a broadband emission in the power range of tens of milliwatts [11,12]. High power operation was also demonstrated using a diode pumped double-clad Tm-doped silica fiber [13]. In this study the authors investigated an asymmetrical cavity feedback to obtain single-ended output, and achieved the highest reported output power of 11 W and with efficiency of 38% by backward ASE (counterpropagating with respect to the pumping power). A theoretical investigation of the ASE in Tm-doped silica fiber with no cavity, i.e., zero feedback on both ends, shows on the other hand that the forward (or copropagating) ASE is expected to be stronger and predicts 30% optical-to-optical conversion [14], whereas experimental results show the opposite. There is no further theoretical study that clarifies this discrepancy between experiment and theory. In addition, there is no theoretical treatment of the inband-pumped ASE in spite of the availability of high-quality measured spectroscopy data of Tm-doped silica fibers that have recently been published [15–17].

In this paper, we present a model of the inband-pumped ASE from Tm-doped silica fiber. We examined a low doping concentration case where no interionic cross-relaxation effects are expected to be present, and therefore we did not include them in our model. The model is based on the two-level rate equation and propagation equations for the pump, forward, and backward ASE signal. The model takes into account the wavelength-dependent absorption and emission cross-sections for two different fiber core compositions. This wavelength dependence impacts the power conversion efficiency, the emission spectral bandwidth, and the ratio of forward versus backward ASE. The results show that with no signal feedback, the backward ASE is considerably stronger in comparison with the forward signal, and it also delivers a broader bandwidth, in agreement with previous experimental observations. Applying asymmetric cavity feedback conditions in the model enables single-ended operation with discrimination of 40∶1 for backward versus forward ASE, as well as decreases the bandwidth by almost 50%. The obtained slope efficiencies were more than 66% in the case with no feedback and more than 70% using the 4% feedback, while the obtained bandwidths were 97 nm and 53 nm, respectively.

2. MODEL

The model of the ASE generation is based on the rate-equation system of electronic excitation in the Tm ions, and propagation equations for the light field in the core of the fiber. The

inband pumping operation is a quasi-three level scheme and with no interionic effects taking place involves only the two lowest lying levels in Tm [4]. Therefore the length-dependent excitation dynamics can be described using the inverted population density N as follows:

$$\frac{\partial N(z,t)}{\partial t} = \int_0^\infty \frac{I_f(\nu,z,t)+I_b(\nu,z,t)}{h\nu}\Gamma[\sigma_a(N_0-N(z,t)) - \sigma_e N(z,t)]\mathrm{d}\nu - \frac{N(z,t)}{\tau}, \quad (1)$$

where $I_{f/b}$ are the spectral intensities of the forward and backward propagating light fields, Γ is the power fill factor, $\sigma_{a/e}$ are absorption and emission cross-sections, N_0 is the number density of the active ions, τ the upper-state level lifetime, ν is the frequency of light, z and t are the spatial and temporal coordinates, and h is the Planck constant. Solving Eq. (1) in the steady-state leads to the following solution for inverted population density:

$$N(z) = \frac{\int_0^\infty \frac{I_f(\nu,z)+I_b(\nu,z)}{h\nu}\Gamma\sigma_a \mathrm{d}\nu}{\int_0^\infty \frac{I_f(\nu,z)+I_b(\nu,z)}{h\nu}\Gamma[\sigma_a+\sigma_e]\mathrm{d}\nu + 1/\tau}. \quad (2)$$

The inverted population can now be calculated from Eq. (2), provided that the two light fields are also known. They can in turn be calculated from their respective propagation equations:

$$\frac{\partial I_{f/b}(\nu,z)}{\partial z} = I_{f/b}(\nu,z)[-\Gamma\sigma_a(N_0-N(z)) + \Gamma\sigma_e N(z) - \gamma(\nu)] + \varrho(\nu)\frac{N(z)}{\tau}. \quad (3)$$

In addition to the absorption and stimulated emission, the light intensities are decreased due to the losses γ, and the spontaneous emission is acting as a source with the power spectral density ϱ, defined as follows:

$$\varrho(\nu) = h\nu g(\nu)\eta\frac{1}{2}[1-(1-NA^2)^{1/2}]. \quad (4)$$

The coefficient $\varrho(\nu)$ depends on the fluorescence lineshape $g(\nu)$ and fluorescent efficiency η, while the last factor is an estimate of the part of the emission captured and guided by the fiber core based on the acceptance solid angle. The core waveguiding properties also determine the power fill factor approximated from

$$\Gamma(\nu) = 1-\exp[-2(a/w(\nu))^2], \quad (5)$$

where a and w are the core and mode-field radii, respectively.

The initial conditions are that all of the ions were in the ground-state, and no light was propagating inside the fiber core as follows:

$$N(z)=0, I_f(\nu,z)=0, I_b(\nu,z)=0. \quad (6)$$

The boundary conditions introduce the pump light at a single frequency $\nu=\nu_p$ as well as cover the partial reflections on both fiber ends as follows:

$$I_f(\nu,z=0) = R_b I_b(\nu,z=0) + I_p(\nu=\nu_p),$$
$$I_b(\nu,z=L) = R_f I_f(\nu,z=L), \quad (7)$$

where R_f and R_b represent the forward and the backward reflected power factors, respectively. The ASE generation model composed of Eqs. (2)–(5) and with the initial and boundary conditions from Eqs. (6) and (7) can be solved by discretization into frequency and spatial intervals and subsequent iteration until the satisfactory convergence of the output parameter happens. Using 200 evenly spaced frequency samples, 100 samples along the fiber length and 500 iteration steps gave accurate results and the execution took only a few seconds for a single run on a personal computer. Spectroscopic data were taken from Agger *et al.* [16], where the authors measured and reported the absorption and emission cross-sections of Tm. Figure 1 shows the absorption and emission cross-sections used in the model and the related transitions. Two sets of data are provided, corresponding to two different fiber core compositions: Al-codoped fiber is designated as Tm1, and Al/Ge-codoped fiber is designated as Tm2. The reported Tm number densities in Agger *et al.* are $8.4\cdot10^{19}$ cm^{-3} and $6.1\cdot10^{19}$ cm^{-3}, respectively, but here a single $N_0=7\cdot10^{19}$ cm^{-3} was chosen for both Tm1 and Tm2 cases to make the comparison more straightforward. The same authors also measured the fluorescence lifetimes of 650 μs for Tm1 and 560 μs for Tm2, and determined the fluorescence efficiency to be 10% in both cases. The same fluorescence data was used in the model here. As no fiber mode parameters were given in [16], our investigation was based on the following parameters from commercially available products from Nufern, Inc. for both fibers, Tm1 and Tm2: 9 μm core diameter and 0.15 NA. The fiber length was set to 90 cm to allow adequate pump absorption in the examined power range. The frequency interval was chosen to span the whole measured cross-section data, between the corresponding wavelengths of 1600 nm and 2050 nm, thus making the spectral resolution of the calculation about 2 nm. The pumping wavelength was set to 1575 nm, losses were set to 10^{-4} cm^{-1} [4], and the feedback from the fiber ends' reflection was set to 0 unless noted otherwise.

3. RESULTS

Using the model presented in the previous section with the experimental data from Agger *et al.*, the pump absorption

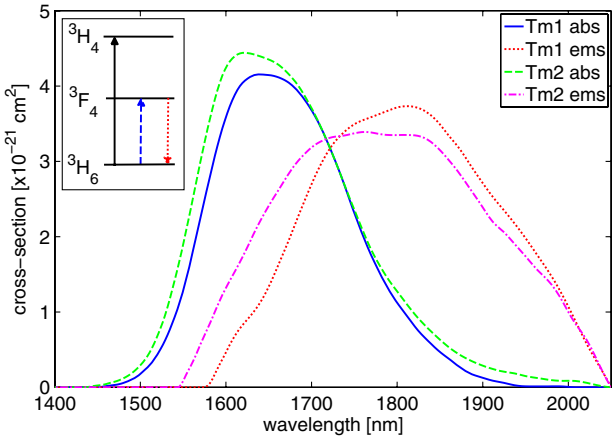

Fig. 1. (Color online) Absorption and emission cross-sections for Tm1 and Tm2 fiber core compositions [16]. Inset shows diode pumping (solid black line), inband pumping (blue dashed), and ASE (red dotted) transitions in Tm.

and signal absorption and emission along the Tm-doped fibers were calculated. Figure 2 shows the resulting pump and ASE power distributions along the length of the fiber core for the Tm1 composition at 500 mW input (launched) pump power. The nonexponential decay of the pumping power is caused by the bleaching of the ground state. Both forward and backward ASE emerge with an exponential-like rise along the length, but the forward ASE is subject to strong reabsorption in the rightmost region of the fiber where the inverted population is not large enough. With increasing pumping powers the peak in the power of the forward ASE is transferred to the right, whereas the backward ASE becomes more powerful. Qualitatively the same behavior results with the Tm2 fiber.

In Fig. 3 the calculated spectra for forward and backward ASE are shown for both fiber compositions. The backward ASE is more powerful and has broader spectrum in both fibers, Tm1 and Tm2. The backward ASE is also blue-shifted in comparison with the forward ASE. There is some difference between the two fibers: in Tm1 fiber the forward and backward ASE have full-width half-maximum (FWHM) of 68 nm and 82 nm, respectively, whereas in Tm2 fiber the FWHM are 80 nm and 98 nm. The 20% broader backward ASE output spectrum compared to the Tm1 composition comes from the broader emission cross-section of Tm2 fiber (see Fig. 1). The Tm2 composition is thus more suited for broad bandwidth needs.

In Fig. 4 the calculated ASE output powers versus input pump powers are shown for both directions and fiber compositions. With respect to the forward ASE, the backward ASE has greater slope efficiency in both fibers. An extrapolation to zero signal of the linearized slope that occurs at high pump powers leads to the definition for the thresholds. This results in 501 mW and 466 mW for the threshold for forward and backward ASE in the Tm1 fiber, respectively, and 599 mW and 513 mW in the Tm2 fiber. The respective slope efficiencies are 24% and 42% in Tm1, and 26% and 34% in Tm2 fibers. The Tm1 composition is better than Tm2 for efficiency, where the overall slope efficiency of combined forward and backward signals is 66% for Tm1 compared to the 60% for Tm2 fiber. The total power conversion efficiencies at 1000 mW input pump power are 39% and 27% for Tm1 and Tm2 fibers, respectively.

The backward propagating ASE has a broader bandwidth and a higher slope efficiency than the forward propagating

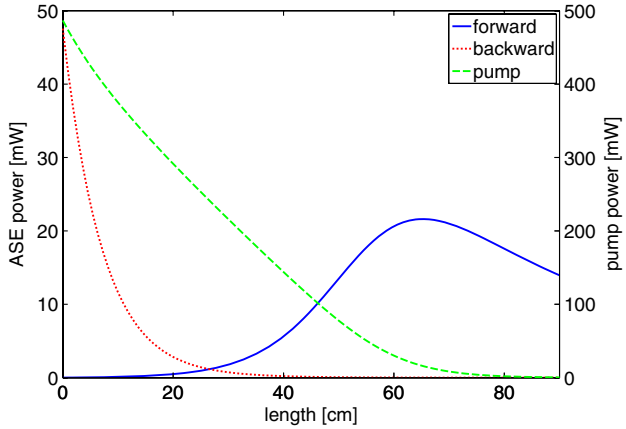

Fig. 2. (Color online) Power distribution along the Tm1 fiber length for the pump, the forward ASE, and the backward ASE.

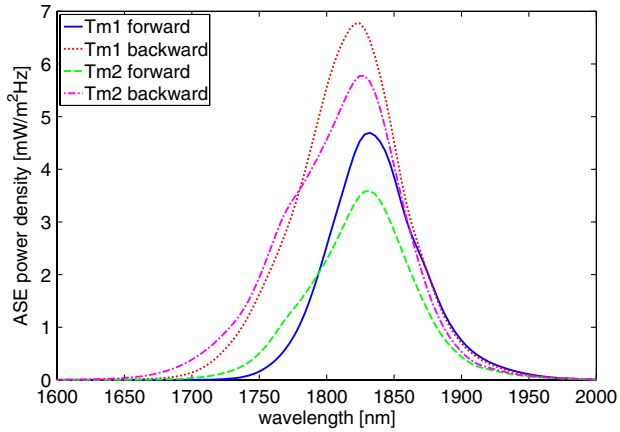

Fig. 3. (Color online) Intensity spectra of the forward and backward ASE for Tm1 and Tm2 fibers. All are at 900 mW input pump power, except the Tm1 backward ASE is at 750 mW input pump power for better comparison.

ASE (see for example Figs. 3 and 4). However, the forward ASE still has ~30% of the combined power in both fiber compositions. In many applications, it is desirable to extract most of the available power from one end of the fiber. One way of achieving this is to extend the length of the fiber. Figure 5 shows ASE power for both directions as well as the ratio of the backward/forward ASE power. When the fiber length is increased over the optimal length determined by the pump absorption, the forward ASE is reabsorbed in the nonpumped region. Part of that power is then transformed to the backward ASE, thus increasing the ratio. The power of the backward ASE is also decreasing because of the losses in the fiber, and an additional drawback of such an approach is that it requires using more than optimal fiber lengths.

Another compelling way to achieve higher ratio of the backward versus forward ASE output power is by imposing an asymmetric cavity condition, e.g., by using a 4% broadband Fresnel reflection on one fiber end, as was recently demonstrated by Shen *et al.* [13]. Figure 6 shows the backward and the forward ASE and its dependence on the pumping power with such feedback, i.e., when $R_b = 4\%$. Inset shows the effect of introduction of the feedback on the ratio of backward/forward ASE power for fiber Tm1. In both fibers the backward ASE is much stronger than the forward ASE at low pumping powers, the ratio being 5:1 for Tm1 and 15:1

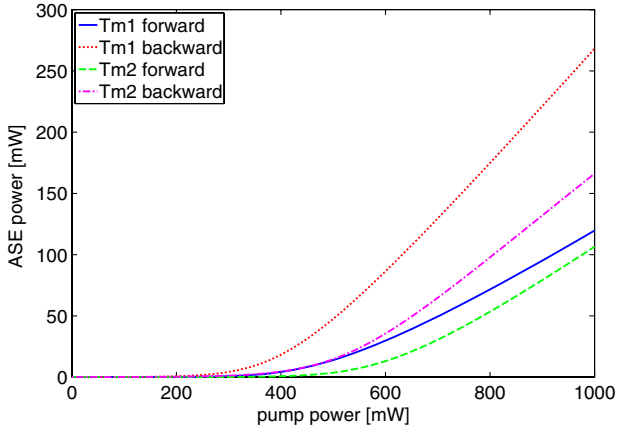

Fig. 4. (Color online) ASE output power versus input pump power for both directions and both fiber compositions with no feedback.

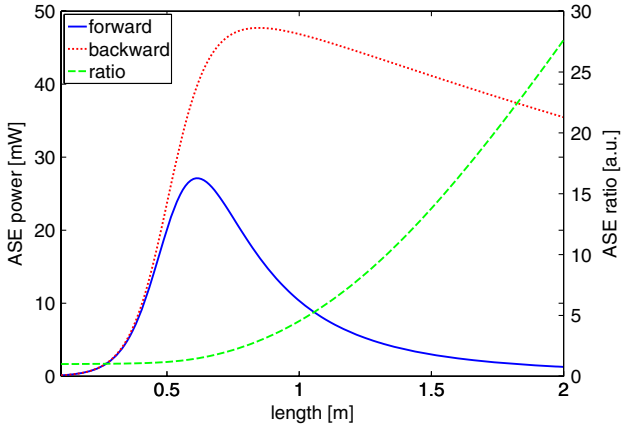

Fig. 5. (Color online) Forward and backward ASE power versus length of the Tm1 fiber at 500 mW input pump power, and the backward/forward ratio of power.

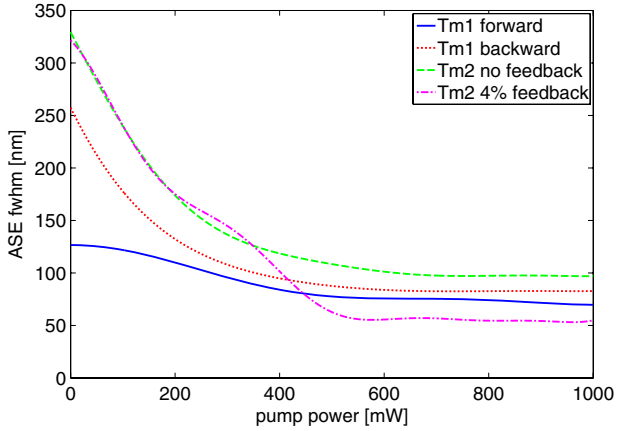

Fig. 7. (Color online) Bandwidth of forward and backward ASE for Tm1 fiber, and the effect of the feedback via $R_b = 4\%$ broadband reflection on the backward ASE for Tm2 fiber.

for Tm2, respectively, but with increasing pumping power the ratio goes down to only 2.2 and 1.6 at high pumping powers. The addition $R_b = 4\%$ broadband reflection feeds back the forward ASE to seed the backward ASE and thus boosts the ratio to 40∶1 and 34∶1 for Tm1 and Tm2, respectively. In addition to that, the slope efficiency of the combined power of backward and forward ASE is increased to 71% for Tm1 and to 70% for Tm2 fibers, respectively.

Using the asymmetric cavity's feedback to boost the power of the backward ASE, however, has a secondary effect in decreasing its bandwidth at high pump powers. Figure 7 shows the bandwidth of the forward and the backward ASE for Tm1 fiber with and without the feedback. The bandwidth at low powers is nearly independent of the presence of the feedback, and both decrease substantially close to the threshold. The decrease is much steeper with respect to the increasing pumping power with the feedback, but it becomes stable, i.e., power independent, at higher powers in both cases. The backward ASE for Tm2 fiber at pumping power of 1000 mW has a FWHM of 97 nm without feedback and only 53 nm with the feedback, respectively, which is even less than the 70 nm FWHM of the forward ASE for Tm1 fiber. The FWHM of the Tm1 fiber with the feedback is also 53 nm (not shown).

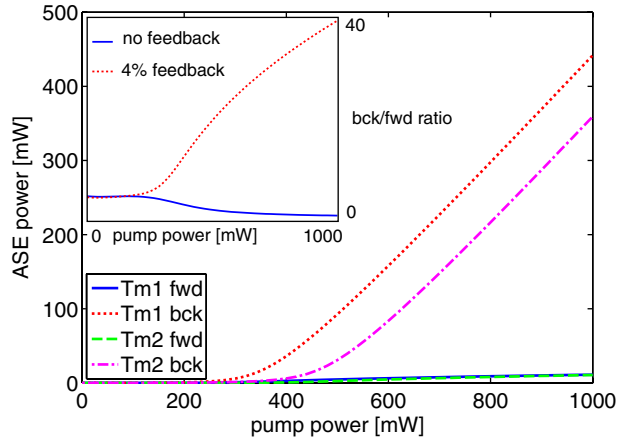

Fig. 6. (Color online) ASE output power versus input pump power for both directions and both fiber compositions with $R_b = 4\%$ broadband reflection. Inset shows the backward/forward ratio of power for Tm1 fiber without and with 4% feedback.

4. DISCUSSION

The comparison between the two different fiber core compositions, namely Al-codoped Tm1 and Al/Ge-codoped Tm2, shows that the first fiber has 10% higher relative slope efficiency while the latter has 18–20% broader bandwidth. The higher efficiency of the Tm1 fiber is caused by its longer fluorescence lifetime, which is 650 μs versus 560 μs in Tm2 fiber. The broader bandwidth of the Tm2 fiber is, on the other hand, caused by the broader stimulated emission cross-section of the Tm2 fiber. This comparison demonstrates that such a model of the ASE generation, and possibly also laser and amplifier operation, is quite sensitive to the underlying spectroscopy data, and confirms the need for meticulous measurements such as those performed in [16,17].

The slope efficiencies of both studied fibers are relatively high, close to the Stokes limit that was nearly attained experimentally with inband pumping of Tm-doped fiber laser oscillators [8–10]. The output signal power is, however, split between the backward and forward propagating ASE by a ratio of about 2∶1. Without any signal feedback the backward ASE is shown to be more prominent in both fibers and for all pumping powers. This is in contrast with the theoretical results in Yu *et al.* [14], although they studied the case with high doping concentrations and with 800 nm pumping, which involves higher lying levels in Tm and the cross-relaxation process between individual ions. However, that change should only affect the population inversion of the model in Eqs. (1) and (2) in addition to the much higher absorption cross-section at 800 nm compared to the 1575 nm. Still, the main factor in the competition between the forward and backward ASE for the inverted population would remain the same, and we believe that backward ASE might be more prominent in that case as well.

The idea of asymmetric cavity feedback indeed provides the solution to obtain a single-ended ASE output in this case as well. Our results show that applying a 4% feedback in the backward direction of the pump propagation results in the discrimination of backward versus forward ASE to 40∶1 at the maximum pumping power that we used. Doing the opposite, i.e., promoting the forward ASE, yields a ratio of only 1∶17. In fact, Shen *et al.* reported very similar numbers, 42∶1 and 1∶23, even though they employed diode pumping at 800 nm and

used highly doped double-clad fibers. This fact might be evidential of the irrelevancy of the underlying pumping scheme in the competition between the generation of the forward and the backward ASE signals. Using the asymmetric cavity feedback also seems to render any differences in the output of the two studied fiber compositions all but negligible.

In addition to the higher efficiency, the backward ASE is also shown to have substantially wider bandwidth than the forward ASE. At low powers, below the threshold of high efficiency of operation, the calculated FWHM spans over 300 nm for Tm2 fiber, and at high power it shrinks considerably, down to 97 nm. It then remains stable and largely independent of the pumping power (see Fig. 7), which is very desirable for its prospective applications. However, the use of an asymmetric feedback to promote the output of the backward ASE also causes the bandwidth to shrink even more at high powers, down to 53 nm for Tm2 fiber. In this latter case again the numbers are roughly comparable to the experimental results from Shen *et al.*, where they reported the bandwidth to go from 280 nm at low pump powers down to 42 nm at highest pump power [13]. Qualitatively similar findings were reported for an ASE in Yb-doped silica fiber, which is also an inband pumped quasi-three level system [18].

5. CONCLUSION

We have presented a model of the amplified spontaneous emission based on solving the rate-equation and light propagation equations of inband-pumped Tm-doped fibers. The results show that the backward propagating ASE has both higher efficiency and wider bandwidth than the forward ASE, which is in good agreement with previously published experimental results. Using the asymmetric cavity feedback to promote backward ASE allowed it to attain 98% of the total output power, but at the expense of losing ~50% of the bandwidth. This should be borne in mind for the prospective applications of the ASE Tm fiber sources near 2 μm. The inband pumping of such sources is expected to deliver comparable efficiencies to the inband-pumped laser oscillation, and also to those already obtained with the more researched diode pumping.

ACKNOWLEDGMENT

This work was financially supported by the Natural Sciences and Engineering Research Council of Canada (NSERC).

REFERENCES

1. T. F. Morse, K. Oh, and L. J. Reinhart, "A new gas detection technique utilizing amplified spontaneous emission light source from a co-doped Tm^{3+} /Ho^{3+} silica fibre in the 2 μm region," Meas. Sci. Technol. **9**, 1409–1412 (1998).
2. B. E. Bouma, L. E. Nelson, G. J. Tearney, D. J. Jones, M. E. Brezinski, and J. G. Fujimoto, "Optical coherence tomographic imaging of human tissue at 1.55 μm and 1.81 μm using Er- and Tm-doped fiber sources," J. Biomed. Opt. **3**, 76–79 (1998).
3. K. Oh, A. Kilian, L. Reinhart, Q. Zhang, T. F. Morse, and P. M. Weber, "Broadband superfluorescent emission of the $^3H_4 \rightarrow {}^3H_6$ transition in a Tm-doped multicomponent silicate fiber," Opt. Lett. **19**, 1131–1133 (1994).
4. S. D. Jackson and T. A. King, "Theoretical modeling of Tm-doped silica fiber lasers," J. Lightwave Technol. **17**, 948–956 (1999).
5. P. Peterka, B. Faure, W. Blanc, M. Karasek, and B. Dussardier, "Theoretical modelling of S-band thulium-doped silica fibre amplifiers," Opt. Quantum Electron. **36**, 201–212 (2004).
6. J. Xu, M. Prabhu, J. Lu, K. Ueda, and D. Xing, "Efficient double-clad thulium-doped fiber laser with ring cavity," Appl. Opt. **40**, 1983–1988 (2001).
7. P. F. Moulton, G. A. Rines, E. V. Slobodtchikov, K. F. Wall, G. Frith, B. Samson, and A. L. G. Carter, "Tm-doped fiber lasers: fundamentals and power scaling," IEEE J. Sel. Top. Quantum Electron. **15**, 85–91 (2009).
8. J. Geng, Q. Wang, T. Luo, S. Jiang, and F. Amzajerdian, "Single-frequency narrow-linewidth Tm-doped fiber laser using silicate glass fiber," Opt. Lett. **34**, 3493–3495 (2009).
9. M. Jiang and P. Tayebati, "Stable 10 ns, kilowatt peak-power pulse generation from a gain-switched Tm-doped fiber laser," Opt. Lett. **32**, 1797–1799 (2007).
10. Y. Tang, F. Li, and J. Xu, "High peak-power gain-switched Tm^{3+}-doped fiber laser," IEEE Photon. Technol. Lett. **23**, 893–895 (2011).
11. Y. H. Tsang, A. F. El-Sherif, and T. A. King, "Broadband amplified spontaneous emission fibre source near 2 μm using resonant in-band pumping," J. Mod. Opt. **52**, 109–118 (2005).
12. Y. H. Tsang, T. A. King, D.-K. Ko, and J. Lee, "Broadband amplified spontaneous emission double-clad fibre source with central wavelengths near 2 μm," J. Mod. Opt. **53**, 991–1001 (2006).
13. D. Y. Shen, L. Pearson, P. Wang, J. K. Sahu, and W. A. Clarkson, "Broadband Tm-doped superfluorescent fiber source with 11 W single-ended output power," Opt. Express **16**, 11021–11026 (2008).
14. G.-Y. Yu, J. Chang, Q.-P. Wang, X.-Y. Zhang, Z. Liu, and Q.-J. Huang, "A theoretical model of thulium-doped silica fiber's ASE in the 1900 nm waveband," Optoelectron. Lett. **6**, 45–47 (2010).
15. B. M. Walsh and N. P. Barnes, "Comparison of Tm:ZBLAN and Tm:silica fiber lasers; spectroscopy and tunable pulsed laser operation around 1.9 μm," Appl. Phys. B **78**, 325–333 (2004).
16. S. D. Agger and J. H. Povlsen, "Emission and absorption cross section of thulium doped silica fibers," Opt. Express **14**, 50–57 (2006).
17. M. Engelbrecht, F. Haxsen, D. Wandt, and D. Kracht, "Wavelength resolved intracavity measurement of the cross sections of a Tm-doped fiber," Opt. Express **16**, 1610–1615 (2008).
18. Q. Xiao, P. Yan, Y. Wang, J. Hao, and M. Gong, "High-power all-fiber superfluorescent source with fused angle-polished side-pumping configuration," Appl. Opt. **50**, 1164–1169 (2011).